Modulated C_{60} monolayers on Si(111)$\sqrt{3}\times\sqrt{3}$-Au reconstructions

A. V. Matetskiy,[1] D. V. Gruznev,[1] A. V. Zotov,[1,2,3] and A. A. Saranin[1,2]
[1]*Institute of Automation and Control Processes, 690041 Vladivostok, Russia*
[2]*Faculty of Physics and Engineering, Far Eastern State University, 690000 Vladivostok, Russia*
[3]*Department of Electronics, Vladivostok State University of Economics and Service, 690600 Vladivostok, Russia*
(Received 26 January 2011; published 9 May 2011)

Adsorption of C_{60} onto the Si(111)-α-$\sqrt{3}\times\sqrt{3}$-Au surface with a high density of domain walls and its In-induced modification, a domain-wall-free Si(111)$\sqrt{3}\times\sqrt{3}$-(Au,In) surface, has been studied using scanning tunneling microscopy (STM). Adsorbed C_{60} have been found to form close-packed hexagonal arrays displaying specific patterns of C_{60} having different dim-bright STM contrast. On the Si(111)-α-$\sqrt{3}\times\sqrt{3}$-Au surface, the dim-bright C_{60} pattern replicates the domain-wall network of the substrate surface and has plausibly an electronic origin. On the homogeneous Si(111)$\sqrt{3}\times\sqrt{3}$-(Au,In) surface, a Moiré pattern of a two-dimensional lattice develops, which indicates periodic occupation of the same regular adsorption sites on the surface. Here, the dim-bright C_{60} contrast is associated plausibly with different topographic heights of the molecules. In the case of the multilayer C_{60} films, the dim-bright C_{60} patterns of the first C_{60} monolayer have been found to be inherited with gradual smearing in the next C_{60} layers.

DOI: 10.1103/PhysRevB.83.195421 PACS number(s): 68.43.Hn, 68.37.Ef, 68.43.Bc

I. INTRODUCTION

Nucleation, growth, and structure of C_{60} monolayers on various surfaces have recently attracted a considerable amount of attention due to their potential use in developing molecular-based devices. Another reason for the research activity in this field is the exceptional variety of phenomena occurring at C_{60} adsorption onto solid surfaces, which presents intriguing puzzles for researchers. The presence of adsorbed C_{60} molecules that display a different scanning tunneling microscopy (STM) contrast (i.e., the observation of the coexisting so-called "bright" and "dim" C_{60}) might serve as an example. The phenomenon has been detected on a number of metal surfaces, particularly on Au(111).[1–3] The difference in the apparent height of the features in STM might result from topographic and/or electronic local variations. It is argued[1,2] that the dim C_{60} molecules arise from the creation of a nanopit in the Au surface below the adsorbed C_{60} molecule, which enhances C_{60}-substrate bonding energy and facilitates charge transfer from the Au(111) surface to C_{60}. Digging nanopits by adsorbed C_{60} is not a peculiarity of only the Au(111) surface, but appears to be a common feature for a variety of metal surfaces, including Au(110),[4] Pt(111),[5] Pt(110),[6] Ag(111),[7] Cu(111),[8] etc. Another general feature for C_{60} adsorption on the vast majority of metal surfaces is that the C_{60} layer often adopts a close-packed hexagonal structure with a C_{60} nearest-neighbor distance close to that of 10.0 Å in a bulk fullerite. This indicates that intermolecular interaction on metal surfaces typically dominates over the fullerene-substrate interaction. In contrast, C_{60} adsorbed on semiconductor surfaces, particularly on Si(111), demonstrates quite a different behavior.[9] The formation of the close-packed molecular monolayers is suppressed there by a relatively strong fullerene-substrate interaction. It is, however, possible to modify the Si(111) surface chemistry by forming an appropriate adsorbate-induced surface reconstruction. For example, highly ordered fullerene assemblies have been grown on the Si(111)$\sqrt{3}\times\sqrt{3}$-Ag reconstruction, and their properties have been characterized in a number of works.[10–14] Thus, adsorbate-induced Si reconstructions are believed to be a promising place to tailor the structure and properties of the adsorbed fullerene arrays. It should be noted, however, that in spite of the great variety of known adsorbate-induced reconstructions on silicon,[15] there have been only a few studies on the fullerene adsorption onto them.[9]Other than fullerenes on Si(111)$\sqrt{3}\times\sqrt{3}$-Ag, which have been studied relatively extensively, we can cite only a few studies on a small number of systems: C_{60}/Si(111)$\sqrt{3}\times\sqrt{3}$-B,[16] C_{60}/Si(111)7 × 7-Co,[17] C_{60}/Bi(0001)/Si(111),[18] and C_{60}/Si(111)1 × 1-Pb.[19]

Here, we present the STM observations of C_{60} adsorption onto the Si(111)-α-$\sqrt{3}\times\sqrt{3}$-Au surface and its In-induced modification, Si(111)$\sqrt{3}\times\sqrt{3}$-(Au,In). The characteristic feature of the first surface is a high density of the domain walls,[20] while the second surface is domain-wall-free.[21] On both surfaces, the adsorbed C_{60} are arranged into the close-packed hexagonal arrays with a nearest-neighbor distance of ∼10.0 Å. Fullerenes within arrays display a different STM contrast (apparent height). The arrangement of the bright and dim C_{60} in the molecular layer produces specific patterns that have been found to be associated with the structural features of the underlying substrate. For the Si(111)-α-$\sqrt{3}\times\sqrt{3}$-Au surface, the patterns reflect the domain-wall network, while for the Si(111)$\sqrt{3}\times\sqrt{3}$-(Au,In) surface, they replicate periodic occupation of the various C_{60} adsorption sites. In the multilayer C_{60} films, the bright-dim C_{60} pattern of the first layer is inherited in the upper layers (up to the fourth layer).

II. EXPERIMENTAL

Our experiments were performed with an Omicron STM operating in an ultrahigh vacuum (∼7.0×10^{-11} Torr). Atomically clean Si(111)7 × 7 surfaces were prepared *in situ* by flashing to 1280 °C after the samples were first outgassed at 600 °C for several hours. Gold was deposited from an Au-wrapped tungsten filament, indium from a Ta crucible, and C_{60} fullerenes from a resistively heated Mo crucible. For STM

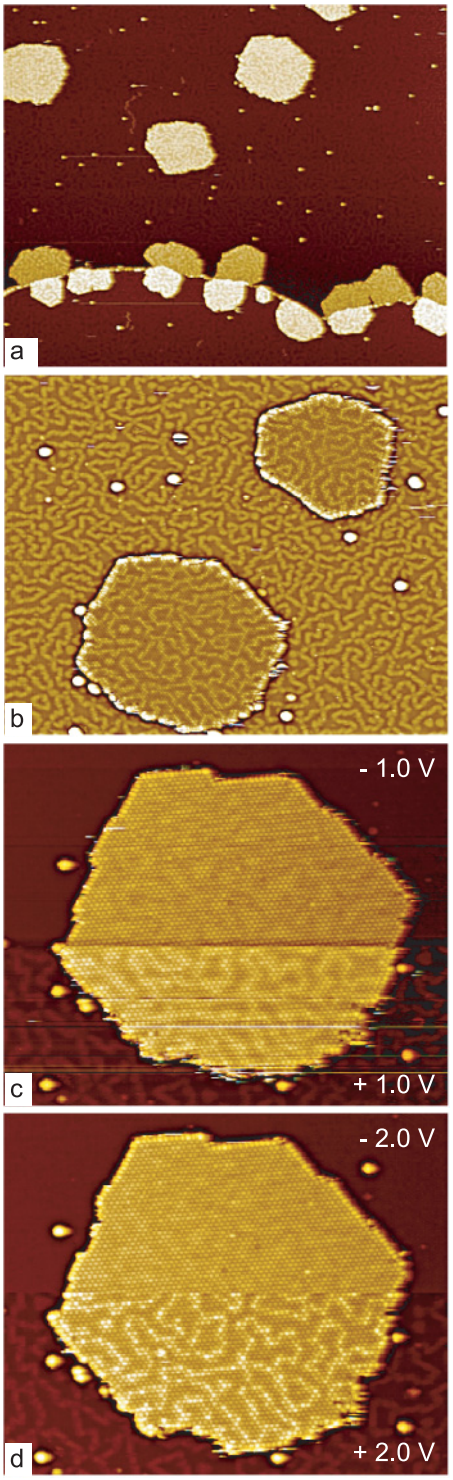

FIG. 1. (Color online) C_{60} arrays forming upon RT adsorption on the Si(111)-α-$\sqrt{3} \times \sqrt{3}$-Au: (a) Large-scale (4000×3300 Å^2) empty-state (+1.5 V) STM image of the surface with 0.02 ML of C_{60}. (b) 1500×1150 Å^2 empty-state (+1.5 V) STM image after applying high-pass Fourier filtering for the better simultaneous visualization of both the substrate and C_{60} island surface structures. 900×700 Å^2 dual polarity (c) $\pm$1.0 V and (d) $\pm$2.0 V STM images of an C_{60} island.

observations, electrochemically etched tungsten tips cleaned by *in situ* heating were employed.

III. RESULTS AND DISCUSSION

Present STM and low-energy electron diffraction (LEED) observations have revealed that C_{60} adsorbed on the Si(111)-α-$\sqrt{3} \times \sqrt{3}$-Au surface demonstrates a behavior similar to that on the metal surfaces. Namely, when deposited onto the surface at RT, the C_{60} molecules form two-dimensional compact islands with preferred nucleation at substrate step edges [Fig. 1(a)]. The C_{60} layer adopts a close-packed hexagonal structure, the periodicity of which coincides with the bulk fullerite nearest-neighbor distance of 10.0 Å within the accuracy of the used LEED and fast Fourier transform (FFT) techniques. The basic translation vectors for most of the hexagonal C_{60} arrays are aligned along the principal crystallographic directions of the Si(111) surface, i.e., $\langle 10\bar{1} \rangle$. However, selected C_{60} arrays rotated by about $\pm 20^\circ$ are also present on the surface. Except for these two types, no other C_{60} arrays have been reliably detected in the numerous experiments.

A peculiar feature of the C_{60} arrays is the presence of bright and dim fullerenes arranged into specific patterns that resemble the domain-wall structure of an Si(111)-α-$\sqrt{3} \times \sqrt{3}$-Au substrate [Fig. 1(b)]. Much like a substrate, a C_{60} layer consists of the "domains" with C_{60} having similar STM contrast and a network of "domain walls" where C_{60} exhibits an apparently different contrast. In the empty-state STM images, C_{60} in the "domains" is dim and that in the "domain walls" is bright, while in the filled-state images the

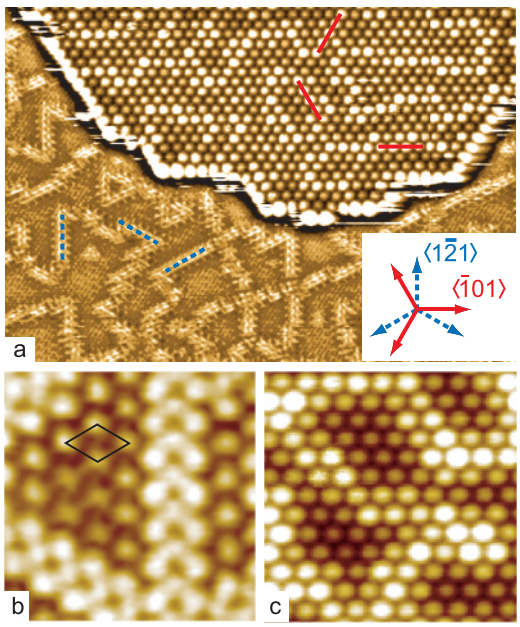

FIG. 2. (Color online) (a) 500×350 high-pass-filtered STM image illustrating orientations of the domain walls at the Si(111)-α-$\sqrt{3} \times \sqrt{3}$-Au surface and those of the bright lines at the C_{60} island. (b) and (c) show these features with a greater magnification: (b) 45×45 Å^2 STM image of the α-$\sqrt{3} \times \sqrt{3}$-Au substrate with outlined $\sqrt{3} \times \sqrt{3}$ unit cell and (c) 100×100 Å^2 STM image of the C_{60} array. The domain walls at the Si(111)-α-$\sqrt{3} \times \sqrt{3}$-Au surface are aligned along the $\langle 1\bar{2}1 \rangle$ directions (indicated by blue dashed bars), while the "domain walls" (bright C_{60} lines) at the C_{60} island are aligned along the $\langle 10\bar{1} \rangle$ directions (indicated by red solid bars).

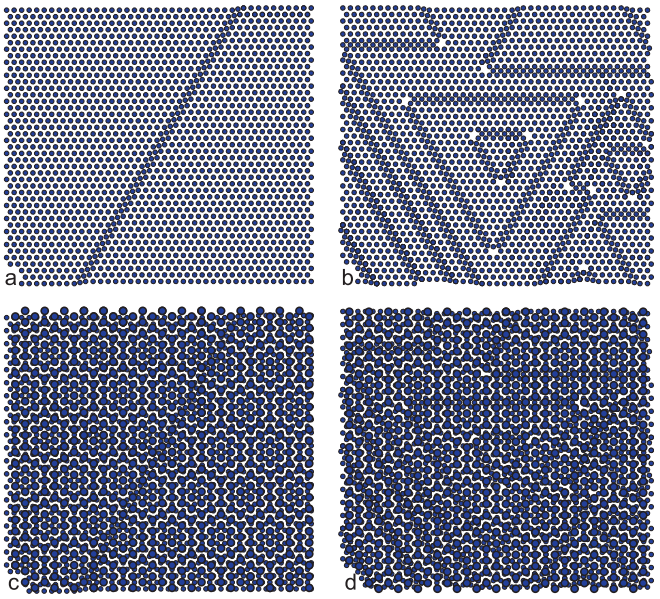

FIG. 3. (Color online) Model simulating appearance of the additional Moiré lines in an adsorbate layer residing atop a substrate with domain walls. (a) Substrate hexagonal array with a single domain wall. (b) Substrate hexagonal array with domain-wall network. (c) and (d) Adsorbate hexagonal array superposed onto the substrate arrays in (a) and (b), respectively.

dim-bright contrast is reversed and less significant [Figs. 1(c) and 1(d)]. Note that commensurate domains of the $\sqrt{3} \times \sqrt{3}$ phase and domain walls at the Si(111)-α-$\sqrt{3} \times \sqrt{3}$-Au surface show the same bias-dependent STM appearance.[20,21] Thus, one can conclude that it is plausible that the dim-bright contrast of fullerenes has an electronic origin, which is dictated by local electronic inhomogeneity at the underlying Si(111)-α-$\sqrt{3} \times \sqrt{3}$-Au substrate surface.

It should be noted, however, that the dim-bright C_{60} pattern does not simply reproduce the underlying domain-wall structure of the substrate (as if the molecular layer would act as a transparent media). Actually, in spite of the seeming similarity, the arrangement of "domain walls" in the C_{60} layer differs from the domain-wall network at the Si(111)-α-$\sqrt{3} \times \sqrt{3}$-Au surface. The principal difference is that the segments of the domain walls at Si(111)-α-$\sqrt{3} \times \sqrt{3}$-Au are always aligned along the $\langle 1\bar{2}1 \rangle$ (i.e., $\sqrt{3}$) directions, while "domain walls" in the C_{60} layer are along the $\langle 10\bar{1} \rangle$ directions (Fig. 2). Thus,

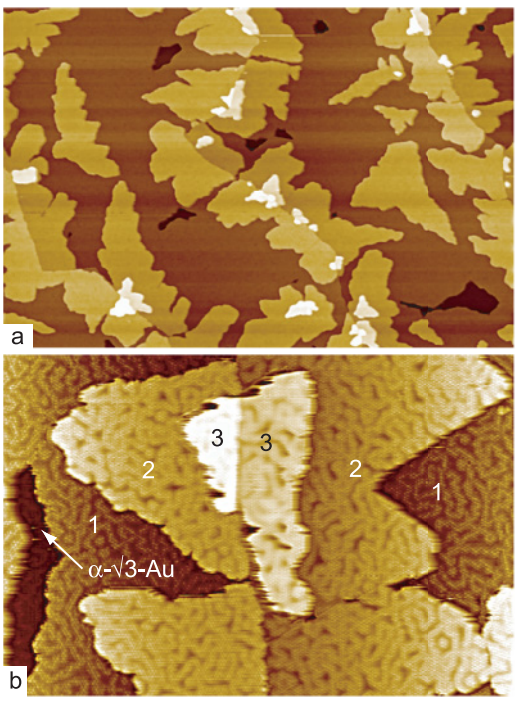

FIG. 4. (Color online) (a) 8000×5300 Å^2 and (b) 1680×1100 Å^2 STM images showing a multilayer C_{00} film grown on the Si(111)-α-$\sqrt{3} \times \sqrt{3}$-Au surface. The uncovered substrate surface is indicated as α-$\sqrt{3}$-Au; first, second, and third C_{60} layers are indicated by 1, 2, and 3, respectively.

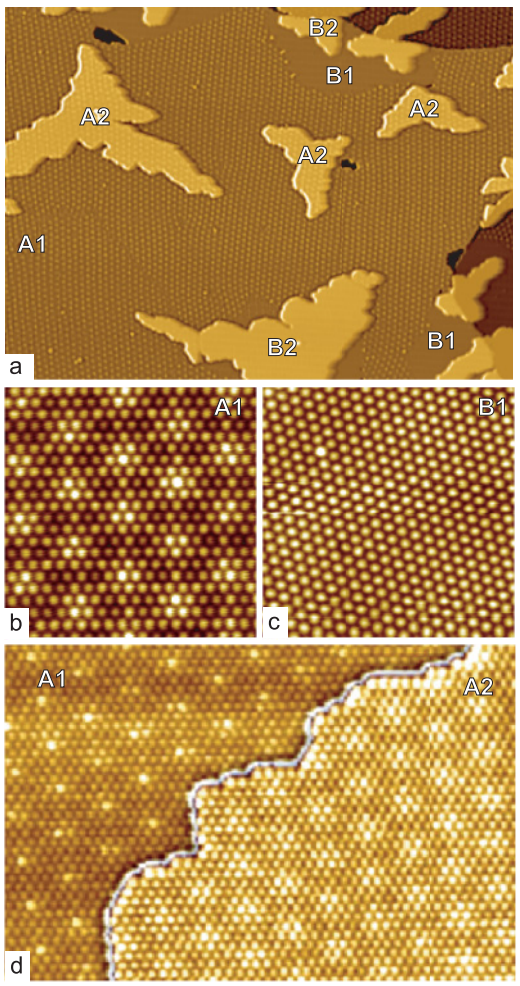

FIG. 5. (Color online) (a) Large-scale (3500×2500 Å^2) STM image showing a two-layer C_{60} film grown at the Si(111)-h-$\sqrt{3} \times \sqrt{3}$-(Au,In) surface at RT. The first-layer and second-layer $\langle 10\bar{1} \rangle$-aligned C_{60} arrays are labeled A1 and A2, respectively. The first-layer and second-layer 20°-rotated C_{60} arrays are labeled B1 and B2, respectively. (b) Close-up (200×200 Å^2) STM image of a type-A1 C_{60} array. (c) Close-up (200×200 Å^2) STM image of a type-B1 C_{60} array. (d) 500×300 Å^2 double-palette-processed STM image illustrating inheritance of the dim-bright C_{60} structure of the first C_{60} A1 layer in the second A2 layer.

the "domain walls" in the C_{60} layer are perpendicular to the domain walls on the Si(111)-α-$\sqrt{3} \times \sqrt{3}$-Au substrate. This observation can be understood with the help of simple model simulations shown in Fig. 3. The figure illustrates the result of superposing a perfect hexagonal adsorbate array onto a hexagonal array of a substrate containing a single domain wall [as in Figs. 3(a) and 3(c)] or a domain-wall network [as in Figs. 3(b) and 3(d)]. One can see that the presence of the substrate domain walls perturbs a regular Moiré pattern by developing additional Moiré lines. These lines are aligned perpendicular to the substrate domain walls, just as in the experiment.

With continuing C_{60} deposition, the next molecular layers overgrow above the first C_{60} layer, thus forming a fullerite film. As an example, Fig. 4(a) shows a surface with an almost completed C_{60} first layer on which the islands of the second layer develop along the substrate step edge. There are also relatively small islands of the third layer atop the second-layer islands. The close-up STM image in Fig. 4(b) of the surface with first-, second-, and third-layer islands clearly shows that the dim-bright C_{60} pattern of the first layer is inherited by the next layers, albeit with a gradual smearing. The pattern is still resolved, at least, up to the fourth molecular layer, indicating the range of the substrate effect on the electronic properties of a fullerite film. This observation could be qualitatively described in terms of Debye screening length. That is, dim-bright bias-dependent STM contrast of C_{60} in the first layer indicates the difference in the charge states of the molecules, which depends on their adsorption sites. Taking into account a semiconducting nature of the fullerite, one could expect quite a sufficient screening length in it, which allows us to resolve at the thin-film surface smeared images of the charges localized in the first layer.

To examine C_{60} growth on a similar Si(111)$\sqrt{3} \times \sqrt{3}$-Au surface that is free of domain walls, we prepared such a surface employing In-induced modification of the original Si(111)-α-$\sqrt{3} \times \sqrt{3}$-Au substrate.[21] That is, ~0.5 ML of In was deposited onto the Si(111)-α-$\sqrt{3} \times \sqrt{3}$-Au at RT followed by a brief annealing at 600 °C, which results in the complete elimination of the domain walls while preserving the original Si(111)$\sqrt{3} \times \sqrt{3}$-Au conjugate-honeycomb trimer (CHCT) structure[22–24] [see Fig. 6(c)]. At the resultant homogeneous surface (h-$\sqrt{3} \times \sqrt{3}$ hereafter), only ~0.15 ML of In is left in the form of a two-dimensional (2D) gas of mobile adatoms[21,25] hopping between adsorption sites indicated in Fig. 6(c) by large blue circles. Taking into account that adsorption sites are separated by a barrier of only ~0.4 eV (Ref. 21), the hopping rate of In atoms at RT exceeds the scanning rate of STM. As a result, RT-STM images display the time-averaging honeycomb

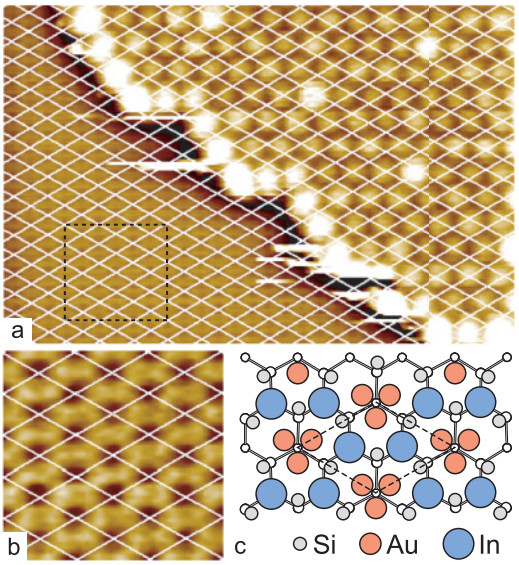

FIG. 6. (Color online) (a) STM image showing 180 × 120 Å^2 surface area with a boundary between the C_{60} array and the Si(111)-h-$\sqrt{3} \times \sqrt{3}$-(Au,In) substrate surface. Hexagonal network is superposed onto the image to tie locations of the bright C_{60} to the h-$\sqrt{3} \times \sqrt{3}$ lattice sites. (b) Enlarged image of the 34 × 34 Å^2 area within a square outlined in (a). One can see that adsorption sites of the bright C_{60} coincide with the hollow depressions in the honeycomb structure of the h-$\sqrt{3} \times \sqrt{3}$ surface. (c) Structural model of the Si(111)-h-$\sqrt{3} \times \sqrt{3}$-(Au,In) surface, where the topmost Si atoms are shown by small gray circles, Au atoms by middle-sized pink circles, and adsorption sites visited by the mobile In atoms by large blue circles. These In atoms are responsible for STM protrusions forming honeycomb structure,[21] hence bright C_{60} resides above Au trimers.

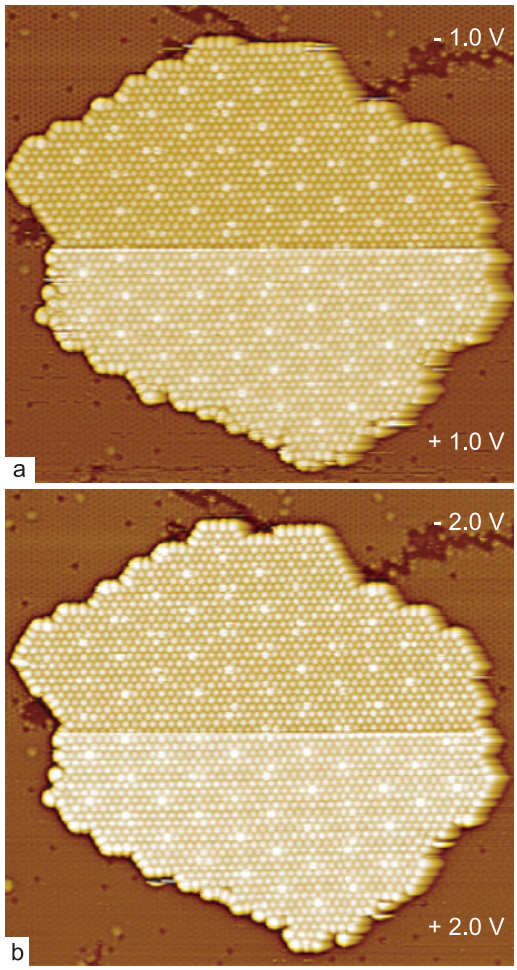

FIG. 7. (Color online) 550 × 500 Å^2 dual polarity (a) ±1.0 V and (b) ±2.0 V STM images of the C_{60} island grown on the Si(111)-h-$\sqrt{3} \times \sqrt{3}$-(Au,In) surface at RT.

pattern, in which all sites are seen as being occupied [see Fig. 6(b)].

C_{60} adsorption onto this surface also results in the formation of the close-packed hexagonal C_{60} arrays, most of which are aligned along the $\langle 10\bar{1}\rangle$ directions, with a few rotated by 20° (Fig. 5). A close inspection of these C_{60} arrays reveals a difference in their appearance: while in the 20°-rotated arrays all C_{60} have a similar STM contrast [Fig. 5(c)], the $\langle 10\bar{1}\rangle$-aligned arrays display a specific dim-bright C_{60} pattern [Fig. 5(b)]. The pattern is of the Moiré type with bright C_{60} forming a nearly perfect 2D lattice.

A hexagonal grid drawn across the boundary between a C_{60} island and the surrounding h-$\sqrt{3}\times\sqrt{3}$ surface allows us to elucidate adsorption sites of the bright C_{60} on the substrate (Fig. 6). One can clearly see that these sites correspond to the hollow depressions in the honeycomb structure of the h-$\sqrt{3}\times\sqrt{3}$ surface. It has been demonstrated in Ref. 21 that STM protrusions in the STM images of h-$\sqrt{3}\times\sqrt{3}$ are due to In atoms visiting T_4 sites, hence hollow depressions are located above the Au trimers, as illustrated in the model in Fig. 6(c). Thus, the bright C_{60} are those residing atop the Au trimers. Their enhanced STM brightness corresponds plausibly to a greater height, taking into account that the contrast of the dim-bright C_{60} pattern is essentially independent of the bias voltage (Fig. 7). Note that the dim-bright C_{60} pattern is inherited in the next C_{60} layers with gradual smearing [Fig. 5(d)]. This behavior is very similar to that of C_{60} on the Si(111)-α-$\sqrt{3}\times\sqrt{3}$-Au surface, although the STM contrast of bright and dim C_{60} in these two cases may very well have a different origin (i.e., topographic and electronic, respectively).

Figure 8 represents a schematic diagram showing the matching of the C_{60} monolayer with the observed dim-bright C_{60} pattern to the underlaying Si(111)$\sqrt{3}\times\sqrt{3}$-Au surface structure. One can see that the translation vector of the C_{60} superlattice $\mathbf{R}$ can be expressed as $\mathbf{R} = 2\mathbf{A}_1 + 3\mathbf{A}_2$ in units of

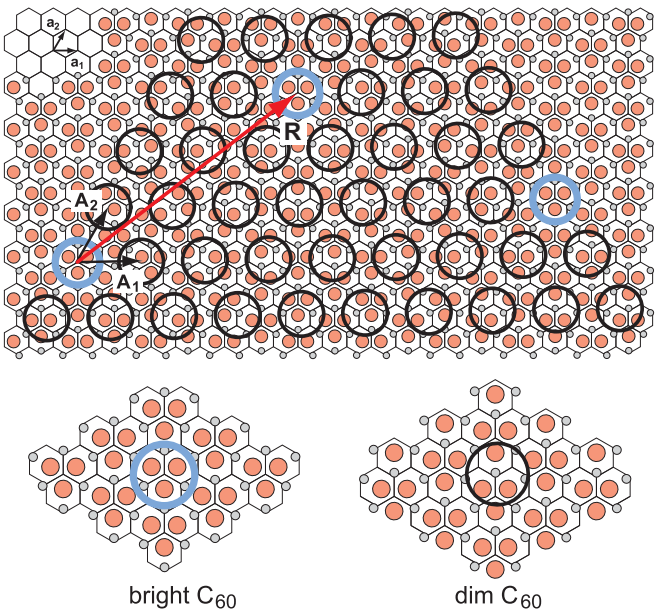

FIG. 8. (Color online) Schematic diagram showing a close-packed C_{60} array superposed onto the ideal Si(111)$\sqrt{3}\times\sqrt{3}$-Au surface with a CHCT structure. Bright C_{60} [outlined by blue (gray) circles] are those located directly above the Au trimers. Basic translation vectors of the Si(111) surface, $\mathbf{a}_1$ and $\mathbf{a}_2$, and those of the C_{60} array, $\mathbf{A}_1$ and $\mathbf{A}_2$, are indicated. The superlattice vector $\mathbf{R}$ connecting two bright C_{60} can be expressed as $5\mathbf{a}_1 + 8\mathbf{a}_2$ or $2\mathbf{A}_1 + 3\mathbf{A}_2$. Note that the C_{60} array is rotated counterclockwise by 1° with respect to the substrate to ensure an ideal lattice matching.

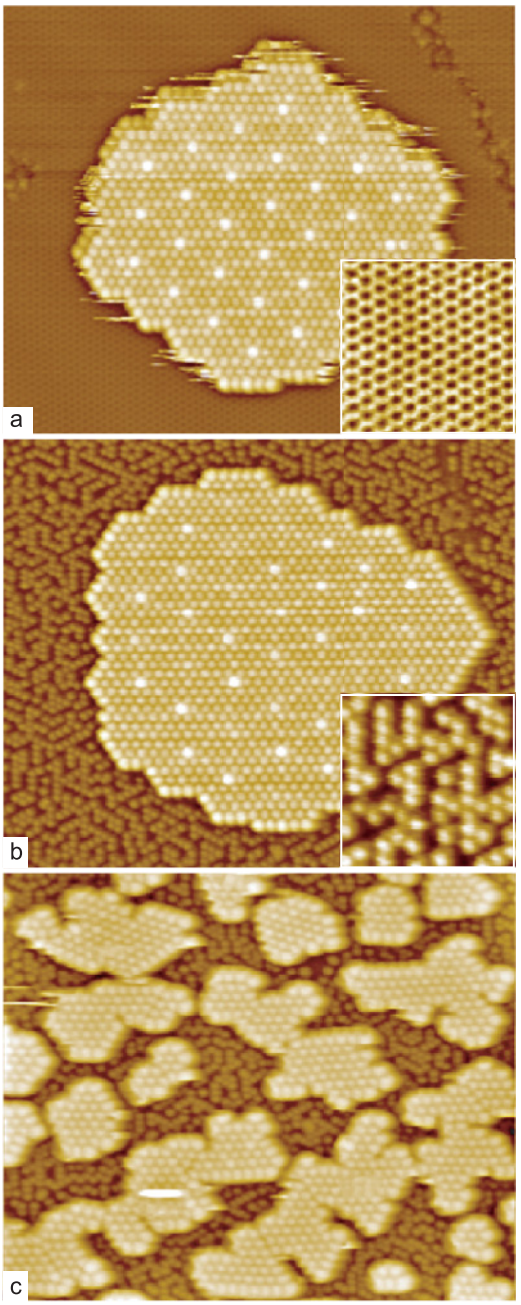

FIG. 9. (Color online) 470 × 470 Å^2 STM images illustrating the appearance of the C_{60} arrays on the Si(111)-h-$\sqrt{3}\times\sqrt{3}$-(Au,In) surface grown and observed under various temperature conditions. (a) A C_{60} island was grown and observed at RT. (b) A C_{60} island was grown at RT, but STM observations were conducted at 115 K. (c) C_{60} islands were grown and observed at 115 K. The insets show the surface structure of the Si(111)-h-$\sqrt{3}\times\sqrt{3}$-(Au,In) surface at (a) RT and (b) 115 K.

the C_{60} lattice constant, $A = 10.0$ Å. The superlattice vector **R** has a length of $\sqrt{19}A = 43.59$ Å. On the other hand, the same vector **R** can be expressed in units of the Si(111) lattice constant, $a = 3.84$ Å as $\mathbf{R} = 5\mathbf{a}_1 + 8\mathbf{a}_2$, and it has a length of $\sqrt{129}a = 43.61$ Å. This evaluation demonstrates that the superlattice of the dim-bright C_{60} pattern and Si(111) lattice is either truly commensurate or very close to being commensurate. It should be noted, however, that actually the rotation angles between **R** and the basic translation vectors $\mathbf{a}_1$ and $\mathbf{A}_1$ are slightly different, being 36.587° for the $\sqrt{19}$ superlattice and 37.589° for the $\sqrt{129}$ superlattice. The accurate angle difference equals 1° 0′ 8″. Thus, for ideal matching, the C_{60} array should be rotated by 1° with respect to the substrate, as illustrated in Fig. 8.

Recall that besides the CHCT Au/Si(111)$\sqrt{3} \times \sqrt{3}$ structure, ~0.15 ML of In adatom gas is present at the h-$\sqrt{3} \times \sqrt{3}$ surface. While the CHCT Au/Si(111) structure apparently controls the formation of the characteristic dim-bright C_{60} pattern in the growing C_{60} monolayer, the role of the 2D gas of mobile In adatoms in this process remains unclear. To clarify this point, we have performed experiments with low-temperature (115 K) STM observations. They have included the LT observations of the C_{60} layers grown at RT, as well as those grown at LT. At LT, thermal motion of In adatoms becomes frozen, and the dynamic honeycomb-like STM appearance of the h-$\sqrt{3} \times \sqrt{3}$ surface [Fig. 9(a)] changes to that of the random array of immobile In adatoms,[21] as one can see in the LT-STM images at the surface in between C_{60} islands [Figs. 9(b) and 9(c)]. Upon cooling the RT-grown C_{60} arrays to LT, the regular dim-bright C_{60} pattern is preserved, albeit with a certain degree of distortion [Fig. 9(b)]. When C_{60} is deposited at LT [Fig. 9(c)], the C_{60} islands are smaller in size but their density is greater compared to the case of RT growth [Fig. 9(a)], due to a lower surface mobility of C_{60}. Another essential peculiarity of the LT growth is the absence of any dim-bright C_{60} pattern at the molecular islands [Fig. 9(c)]. An important note is that the In adatoms do remain under the growing C_{60} island, as the density of In adatoms at the uncovered surface, 0.15 ± 0.02 ML, does not change with the C_{60} layer growth. The above observations imply that the regular dim-bright C_{60} pattern is dictated by the CHCT Au/Si(111) structure, while In adatoms tend to occupy certain hollow sites in between C_{60}, where they would not disturb C_{60} ordering within the molecular layer. At RT, In adatoms are believed to hop dynamically between these sites. Upon cooling to LT, some portion of the In adatoms could be frozen in the intermediate sites, causing a certain distortion in the dim-bright C_{60} pattern. In the case of the LT growth, a solid random array of immobile In adatoms eliminates the ordering effect of the CHCT Au/Si(111) structure, hence no regular dim-bright C_{60} pattern develops at the molecular layer.

IV. CONCLUSIONS

In conclusion, we have found that C_{60} adsorption onto the Au-induced Si(111) reconstructions, the Si(111)-α-$\sqrt{3} \times \sqrt{3}$-Au phase, and its In-induced modification, Si(111)$\sqrt{3} \times \sqrt{3}$-(Au,In), results in developing modulated C_{60} monolayers with specific dim-bright C_{60} patterns in STM images. The origin of these patterns differs from that known for C_{60} monolayers on the Au single-crystalline surfaces, where the appearance of dim C_{60} is typically associated with the creation of a nanopit in the Au surface below the adsorbed C_{60} molecule. In contrast, the reconstructed Au/Si(111) surfaces remain intact upon C_{60} adsorption, and their atomic arrangements control the forming dim-bright C_{60} patterns. In the case of the Si(111)-α-$\sqrt{3} \times \sqrt{3}$-Au surface, the dim-bright C_{60} pattern replicates the domain-wall network of the substrate surface. On the homogeneous Si(111)$\sqrt{3} \times \sqrt{3}$-(Au,In) surface, a Moiré pattern develops, reflecting periodic occupation of the regular adsorption sites on the surface, i.e., bright C_{60} residing atop Au trimers forms the Si(111)$\sqrt{129} \times \sqrt{129}$ lattice. Structural and electronic properties of the first C_{60} monolayer are inherited in the next molecular layers: the smeared dim-bright C_{60} patterns remain resolvable even in the fourth C_{60} layer.

ACKNOWLEDGMENTS

Part of this work was supported by the Russian Foundation for Basic Research (Grants No. 09-02-00094 and No. 09-02-98500) and the Russian Federal Agency for Science and Innovations (Grants No. P1420, No. 02.740.11.0111, and No. 4634.2010.2).

[1] J. A. Gardener, G. A. D. Briggs, and M. R. Castell, Phys. Rev. B **80**, 235434 (2009).
[2] L. Tang, X. Zhang, Q. Guo, Y.-N. Wu, L.-L. Wang, and H.-P. Cheng, Phys. Rev. B **82**, 125414 (2010).
[3] X. Zhang, F. Yin, R. Palmer, and Q. Guo, Surf. Sci. **602**, 885 (2008).
[4] M. Hinterstein, X. Torrelles, R. Felici, J. Rius, M. Huang, S. Fabris, H. Fuess, and M. Pedio, Phys. Rev. B **77**, 153412 (2008).
[5] R. Felici, M. Pedio, F. Borgatti, S. Iannotta, M. Capozi, G. Ciullo, and A. Stierle, Nat. Mater. **4**, 688 (2005).
[6] X. Torrelles, V. Langlais, M. DeSantis, H. C. N. Tolentino, and Y. Gauthier, Phys. Rev. B **81**, 041404 (2010).
[7] H. I. Li *et al.*, Phys. Rev. Lett. **103**, 056101 (2009).
[8] W. W. Pai *et al.*, Phys. Rev. Lett. **104**, 036103 (2010).
[9] P. J. Moriarty, Surf. Sci. Rep. **65**, 175 (2010).
[10] T. Nakayama, J. Onoe, K. Takeuchi, and M. Aono, Phys. Rev. B **59**, 12627 (1999).
[11] K. Tsuchie, T. Nagao, and S. Hasegawa, Phys. Rev. B **60**, 11131 (1999).
[12] M. J. Butcher, J. W. Nolan, M. R. C. Hunt, P. H. Beton, L. Dunsch, P. Kuran, P. Geiorgi, and T. J. S. Dennis, Phys. Rev. B **64**, 195401 (2001).
[13] L. Wang *et al.*, Surf. Sci. **564**, 156 (2004).
[14] G. L. LeLay, M. Göthelid, V. Y. Aristov, A. Cricenti, M. C. Håkansson, C. Giammichele, P. Perfetti, J. Avila, and M. C. Asensio, Surf. Sci. **377/379**, 1061 (1997).

[15]V. G. Lifshits, A. A. Saranin, and A. V. Zotov, *Surface Phases on Silicon* (Wiley, Chichester, 1994).
[16]T. Stimpel, M. Schraufstetter, H. Baumgärtner, and I. Eisele, Mater. Sci. Eng. B **89**, 394 (2002).
[17]M. A. K. Zilani, H. Xu, Y. Y. Sun, X. S. Wang, and A. T. S. Wee, Appl. Surf. Sci. **253**, 4554 (2007).
[18]J. T. Sadowski, R. Z. Bakhtizin, A. I. Oreshkin, T. Nishihara, A. Al Mahboob, Y. Fujikawa, K. Nakajima, and T. Sakurai, Surf. Sci. **601**, L136 (2007).
[19]S. H. Chang, I. S. Hwang, C. K. Fang, and T. T. Tsong, Phys. Rev. B **77**, 155421 (2008).
[20]T. Nagao, S. Hasegawa, K. Tsuchie, S. Ino, C. Voges, G. Klos, H. Pfnür, and M. Henzler, Phys. Rev. B **57**, 10100 (1998).
[21]D. V. Gruznev, I. N. Filippov, D. A. Olyanich, D. N. Chubenko, I. A. Kuyanov, A. A. Saranin, A. V. Zotov, and V. G. Lifshits, Phys. Rev. B **73**, 115335 (2006).
[22]Y. G. Ding, C. T. Chan, and K. M. Ho, Surf. Sci. **275**, L691 (1992).
[23]I. H. Hong, D. K. Liao, Y. C. Chou, C. M. Wei, and S. Y. Tong, Phys. Rev. B **54**, 4762 (1996).
[24]J. Y. Lee and M. H. Kang, J. Korean Phys. Soc. **55**, 2460 (2009).
[25]J. K. Kim, K. S. Kim, J. L. McChesney, E. Rotenberg, H. N. Hwang, C. C. Hwang, and H. W. Yeom, Phys. Rev. B **80**, 075312 (2009).